Synthesis of Large Pore LTL and MOR Zeolites and Use as Adsorbent for The Removal of Heavy Metal and Radioactive Metal Ions in Aqueous Solution

Duy Hoai-Phuong Nguyen
Vietnam National University Ho Chi Minh City
Quang Thanh Le
Vietnam Academy of Science and Technology
Tung Cao Thanh Pham (pcttung@ict.vast.vn)
Vietnam Academy of Science and Technology https://orcid.org/0000-0002-4631-481X
Thanh Tu Le
Vietnam National University Ho Chi Minh City

Research Article

Keywords: Large pore zeolites, porous materials, heavy metal, radioactive, metal adsorption

Posted Date: June 29th, 2021

DOI: https://doi.org/10.21203/rs.3.rs-617526/v1

Synthesis of large pore LTL and MOR zeolites and use as adsorbent for the removal of heavy metal and radioactive metal ions in aqueous solution

Duy Hoai-Phuong Nguyen[a,b], Quang Thanh Le[c], Tung Cao-Thanh Pham[c*], Thanh Tu Le[a,b*]

---

[a]University of Science, Ho Chi Minh City, Dist.5, 72711, Vietnam.

[b]Vietnam National University, Ho Chi Minh City, Vietnam.

[c]Vietnam Academy of Science and Technology, Institute of Chemical Technology, Ho Chi Minh City, Dist.12, 71515, Vietnam.

Corresponding author

*e-mail: letuthanh@hcmus.edu.vn;
pcttung@ict.vast.vn; Tel: +84-(0)93 6863035; Fax: +84-(0)283 8293889

Acknowledgments

This work was supported by Vietnam National University, Ho Chi Minh City, Vietnam for project code No. C2018-18-23. We would like to thank Associate Professor Nguyen Van Dong from Faculty of Chemistry, University of Science, VNU-HCMC for supporting the measurement of heavy metal ion.

Abstract

Heavy metal and radioactive ions can cause serious environmental problems if they are not completely removed from wastewater as well as in groundwater. In this study, large pore LTL and MOR zeolites were successfully synthesized and used as adsorbent to remove Pb^{2+}, Cu^{2+}, Zn^{2+}, Cd^{2+}, Cs^{+} and Sr^{2+} ions in aqueous solution. At low initial concentration (10 ppm), LTL and MOR zeolites effectively removed above metal ions with removal efficiency in the range of 95-99%. Both zeolites showed high affinity to Cs^{+} and Pb^{2+} ions with the adsorption capacity of LTL zeolite to Cs^{+} and Pb^{2+} were 278.8 mg/g and 141.4 mg/g, and that of MOR zeolite were 238.8 mg/g and 178.9 mg/g, respectively. The EDS results showed that Pb^{2+} ions from the aqueous solution were exchanged with exchangeable Na^{+} ions in MOR zeolite and K^{+} ions in LTL zeolite. The pseudo-second-order kinetic model and Langmuir isotherm model fitted better to experiment data on the adsorption of metal ions on both LTL and MOR zeolite. This result revealed that the adsorption of these metal ions on LTL and MOR zeolite was monolayer chemisorption. The equilibrium adsorption results showed that the microstructure of zeolite significantly affected the adsorption capacity of LTL and MOR zeolite on removal of tested metal ions.

Keywords

Large pore zeolites, porous materials, heavy metal, radioactive, metal adsorption

Introduction

Heavy metal pollution is one of the most concerning issues in the balance between industrialization and environment protection. Heavy metal contamination usually comes from heavy industries and manufacturers such as mining, steel, metal plating, tanneries, battery production (Sprynskyy et al. 2006). Heavy metal ions such as lead (Pb^{2+}), copper (Cu^{2+}), zinc (Zn^{2+}), cadmium (Cd^{2+}) are non-biodegradable, highly water-soluble. They permeate into and accumulate for long time in soil, pollute the surface water and ground-water. Due to the bioaccumulation, they can absorb and accumulate in food, living organisms, human bodies and cause serious health effects (Azimi et al. 2017). Besides, radioactive contaminants in nuclear facilities waste stream are also an important environmental concern. Cesium (Cs) and strontium (Sr) are the most abundant radionuclides in nuclear fission products. The radioactive Cs and Sr are very dangerous to human health due to their relatively long half-life, about 30 years. The environmental problem caused by these radioactive isotopes will last for a very long time (El-Kamash 2008).

Several methods and technologies have been developed to eliminate heavy metals and radioactive metals in waste water prior to discharge. Some of the common methods are electro-coagulation, electro-flotation, electrodeposition, chemical precipitation, ion exchange, adsorption, membrane filtration, reverse osmosis, and advance oxidation (Azimi et al. 2017). Among these methods, adsorption is one of the most popular techniques due to its simplicity and efficiency.

Zeolite is a microporous material with a well-defined framework and microstructure. Depending on composition and microstructure, zeolites have different micro-properties and applications (Lobo 2003). In adsorption application, the pure silica zeolite with hydrophobic channel system showed high capture capacity to radioactive iodine (Pham et al. 2016). Some synthetic zeolites were reported with very high selectivity in removal of radioactive metal ions (Datta et al. 2014, 2019). Aluminosilicate zeolites are suitable for removal of metal ions from water due to their high porsosity, hydrophilic channel system, high stability, high ion exchange capacity, and their ability to generate non-toxic counter exchanged-ion (Davis 2014, Zendelska et al. 2014). Natural zeolites have been widely studied for the removal of metal ions in aqueous solution. Among natural zeolites, clinoptilolite and mordenite were the most concerned. They were used as adsorbent for the removal of heavy metal ions such as Pb^{2+}, Cu^{2+}, Zn^{2+}, Co^{2+}, Mn^{2+} in aqueous solution (Sprynskyy et al. 2006, Zendelska et al. 2014, Erdem et al. 2004, Günay et al. 2007, Wang et al. 2008, Mihaly-Cozmuta et al. 2014, Aghel et al. 2020, Galletti et al. 2020). Clinoptilolite and mordenite natural zeolites were also used for

decontamination of radioactive ions as Cs^{+}, Sr^{2+}, Co^{2+} (Moattar and Hayeripour 2004, Prajitno et al. 2021). Clinoptilolite is found naturally in the form of rock. It contains several impurity phases such as quartz, smectite, mica (Wang et al. 2008). Therefore, the adsorption capacity of natural zeolites is highly different from reported works, varied from a few to hundreds of mg/g, depending on the sources of the zeolites (Sprynskyy et al. 2006, Erdem et al. 2004, Wang et al. 2008). Synthetic zeolites have been used in catalytic reaction, gas separation, sensing material, wastewater treatment (Kwon et al. 2020). Among various zeolite frameworks, Linda Type A (LTA) zeolite has the lowest silicon-aluminum ratio, Si/Al of 1-2, leading to the highest cation exchange capacity (Collins et al. 2020). Synthetic LTA zeolite was used as adsorbent material for the removal of heavy metal and radioactive metal ions from aqueous solution (El-Kamash et al. 2005, Ibrahim et al. 2010, Tashauoei et al. 2010, Lu et al. 2016, Shen et al. 2017, Hong et al. 2019, Li et al. 2020). Despite its remarkable cation exchange capacity, the small-pore of LTA zeolite, with the pore diameter of 4.1 Å, may affect their metal ions removal efficiency (Kwon et al. 2020).

Linda Type L (LTL) and mordenite (MOR) zeolites are two of the most widely used large-pore synthetic zeolites. The crystal structure of LTL zeolite consists of a one-dimensional channel with aperture of about 7.1 Å running across the *c*-axis (McCusker et al. 2007), and the Si/Al ratio ranging of 3.0-6.0 (typically 3.0). LTL zeolite is mostly used as catalyst (Calzaferri 2020), host for accommodation of organic dye as optical material (Calzaferri 2020, Fois et al. 2013). MOR zeolite is a two-dimensional channel system with Si/Al ratio in the range of 4-12. The framework of MOR zeolite contains an elliptical pore channel with pore size of 6.7×7.0 Å running across the *c*-axis and another channel running across the *b*-axis with pore diameter of 2.6×5.7 Å (McCusker et al. 2007). MOR zeolite has been used in catalytic reactions, semiconductors, chemical sensors, separation of gas or liquid mixture, and solid adsorbent (Hincapie et al. 2004).

We report here the synthesis of large pore LTL and MOR zeolite by conventional hydrothermal reaction and use of synthesized zeolites as adsorbent for removal of heavy metal ions including Cu^{2+}, Cd^{2+}, Pb^{2+}, Zn^{2+}, and radioactive ions including Cs^{+}, Sr^{2+} in aqueous solution. The sorption characteristics including adsorption kinetic, adsorption equilibrium and sorption models were investigated.

Materials and methods

Materials

Aluminum hydroxide ($Al(OH)_3$, 76.5%, Alfa Aesar), Potassium hydroxide (KOH, 85%, Merck), Sodium aluminate ($NaAlO_2$, 99%, Alfa Aesar), Sodium hydroxide (NaOH, 99%, Merck), Ludox-AS40 (SiO_2, 40%, Sigma Aldrich) were used for the synthesis of

LTL and MOR zeolites. Cadmium acetate ($(CH_3COO)_2Cd.2H_2O$, >99%, Xilong Scientific), Copper(II)nitrate ($Cu(NO_3)_2.2H_2O$, >99%, Xilong Scientific), Lead(II)nitrate ($Pb(NO_3)_2$, >99%, Xilong Scientific), Zinc sulfate ($ZnSO_4.7H_2O$, >99%, Xilong Scientific), Caesium nitrate ($CsNO_3$, >99%, Xilong Scientific), Strontium nitrate ($Sr(NO_3)_2$, >99%, Xilong Scientific) were used in metal removal experiments. All chemicals and reagents in this study were used as received without further purification.

Synthesis of LTL and MOR zeolite

LTL zeolite was synthesized from a gel composed of KOH, $Al(OH)_3$, Ludox-AS40 and deionized water (DIW) with the molar ratio in term of $Al_2O_3/K_2O/SiO_2/H_2O$ was 1.2/3.0/9.83/165. The reaction gel was prepared by adding 1.32 g of KOH and 6.62 g of DIW in a plastic beaker with stirring until completely dissolved, then 0.82 g of $Al(OH)_3$ was added. After stirring for 30 minutes at room temperature, 4.82 g of Ludox-AS40 was added dropwise into the solution to create a white gel. The gel was aged for 3.5 hours at room temperature with vigorous stirring. The reaction gel was then transferred into a Teflon-lined autoclave. The hydrothermal reaction was carried out in a conventional oven at 170°C for 3 days.

MOR zeolite was synthesized from a gel composed of NaOH, $NaAlO_2$, Ludox-AS40 and DIW with the molar ratio in term of $Na_2O/Al_2O_3/SiO_2/H_2O$ was 4.5/1/19/294. The synthesis gel was prepared by adding 0.63 g of NaOH and 7.8 g of DIW in a plastic beaker with stirring until completely dissolved, then 0.37 g of $NaAlO_2$ was added. The mixture was stirred for 30 minutes to create a homogenous white color mixture. After that, 6.3 g of Ludox-AS40 was added dropwise into the mixture to obtain a white gel. The gel was aged for 2 hours at room temperature with vigorous stirring. The synthesis gel was then transferred into a Teflon-lined autoclave. The hydrothermal reaction was carried out in a conventional oven at 175°C for 4 days.

Sorption studies

Kinetic study

Kinetic adsorption of metal ions on zeolite was investigated by adding 0.1 g of LTL/MOR zeolite and 150 mL solution containing 50 ppm of single metal ions as Cu^{2+}, Cd^{2+}, Pb^{2+}, Zn^{2+}, Cs^{+}, Sr^{2+} into a glass beaker. The pH of the solution was about 6.0 – 7.0. The mixture was then stirred at room temperature. After certain periods of time, 2 mL of the aliquot was collected whilst the mixture was kept stirring to maintain the initial ratio of adsorbent and solution. Zeolite adsorbent in the collected sample was separated by centrifugation, and the concentration of metal ions in the solution was measured.

The adsorption capacity and the removal efficiency of zeolite for metal ions were calculated using the equation (1) and (2), respectively:

$$q = \frac{(C_0 - C_t)\, x\, V}{m} \qquad (1)$$

$$H = \frac{(C_0 - C_t)}{C_0} \qquad (2)$$

where t (minute) was time length of the adsorption test, C_0 (ppm) and C_t (ppm) were the concentrations of metal ions in the initial solution and the solution at time t, respectively, m (g) was the weight of zeolite adsorbent, V (L) was the volume of the solution, q (mg/g) was the adsorption capacity and H (%) was the removal efficiency.

Equilibrium study

Batch adsorption experiment was carried out at room temperature in 250 mL glass beaker with using 0.1 g of LTL/MOR zeolite and 150 mL of metal salt solution containing single metal ions as Cu^{2+}, Cd^{2+}, Pb^{2+}, Zn^{2+}, Cs^{+}, Sr^{2+}. The initial concentration of metal ions was varied from 10 to 600 ppm. The pH of the solution was about 6.0-7.0. The mixture was stirred for 2 hours (in case of LTL zeolite) or 3 hours (in case of MOR zeolite) for saturated adsorption. After adsorption time, zeolite was removed from the solution by centrifugation, and concentration of metal ions remaining in solution was determined. The adsorption capacity and removal efficiency were calculated as described above.

Characterization methods

Scanning electron microscopy (SEM) analysis was obtained from scanning electron microscope JEOL JSM-6400 operating at acceleration voltage of 5 kV. Powder X-ray diffraction (XRD) patterns were obtained using a Bruker D8 Advance powder X-ray diffractometer operating at 40 kV and 40 mA with Cu–Kα radiation. Energy dispersive X-ray (EDS) measurements were obtained from Hitachi FESEM S4800 and Horiba EDX H-7593. The concentrations of heavy metal ions were measured using a flame-atomic absorption spectrophotometry (Shimadzu AA-6300) with an air-acetylene flame. Cadmium, copper, cesium, lead, strontium and zinc hollow cathode lamps were used as radiation source with wavelengths of 228.8 nm, 852.1 nm, 324.8 nm, 283.3 nm, 460.7 nm, respectively.

Result and discussion

Characterization of synthesized zeolites

We first synthesized two types of large pore LTL and MOR zeolite by conventional hydrothermal reaction as described in detail in the experiment section, and their characteristics were shown in Fig. 1. The typical hexagonal prism crystals of LTL zeolite were obtained by scanning electron microscope (SEM) as shown in Fig. 1a. The x-ray diffraction pattern (XRD) in Fig. 1b confirmed the main LTL zeolite structure in the synthesized product. Similarly, MOR zeolite with average crystal size of 20 μm and prismatic morphology was synthesized and shown in Fig. 1c. The XRD pattern showed the peaks of MOR structure (Fig. 1d). The relatively high intensity diffraction peaks are consistent with the large crystal, and reveal the high crystallinity of obtained material. The Si/Al ratio obtained by energy dispersive spectroscopy (EDS) measurements were 2.97 for LTL and 6.91 for MOR zeolite, respectively. The above synthesized LTL and MOR zeolites were used as adsorbent for heavy metal removal studies without further modification.

Kinetic studies

In this work, the effect of adsorption time to the adsorption of metal ions on LTL zeolite was shown in Fig. 2. The adsorption process of all metal ions on LTL zeolite was relatively fast. Within 15 minutes, the equilibrium state was reached (except Sr^{2+}, the equilibrium was reached at 60 minutes). The pseudo-first-order and pseudo-second-order models of the metal ions adsorption on LTL zeolite were also presented in Fig. 2. The parameters of these models are shown in Table 1. The correlation coefficients R^2 of pseudo-second-order model (0.99-1) were much higher than that of the pseudo-first-order model case (0.21-0.79), and the simulated equilibrium adsorption capacity calculated from pseudo-second-order model was approximate to the experimental data (Fig. 2a-f). Therefore, the pseudo-second-order model was more suitable to describe the adsorption kinetic of metal ions on LTL zeolite (Fig. 2g,h). The obtained result revealed that the pseudo-second-order sorption mechanism was predominant, and the adsorption rate of metal ions on LTL zeolite occurred following the chemisorption process (El-Kamash et al. 2005).

Additionally, the adsorption of metal ions on MOR zeolite with different periods of time was shown in Fig. 3. The adsorption process of Pb^{2+} and Cs^{+} ions on MOR zeolite occurred relatively faster than that of the remaining metal ions (Fig. 3a,b). The equilibrium state achieved within 10 minutes, whilst the adsorption process and the loading amount of Cu^{2+}, Cd^{2+}, Zn^{2+}, Sr^{2+} metal ions on MOR zeolite kept increasing slowly until 180 minutes of adsorption experiment without getting equilibrium state (Fig. 3c-f). The pseudo-first-order and pseudo-second-order models of the metal ions adsorption on MOR zeolite were plotted in Fig. 3a-f, and the parameters of these models were presented in Table 2. Similar to the LTL zeolite case, the pseudo-second-order

model fitted with higher fitting degree to experiment data on kinetic adsorption of metal ions on MOR zeolite (Fig. 3g,h). The chemisorption was the main process governing the sorption rate of tested metal ions on MOR zeolite.

The calculated pseudo-second-order model adsorption rate constants k_2 of metal ions on LTL, MOR zeolite were shown in Table 3. The adsorption rate constants of tested metal ions on LTL zeolite were higher than the obtained values in MOR zeolite case. In our study, there are two factors that might affect to this result, including the Si/Al ratio and crystal size of two zeolites. The LTL zeolite with Si/Al ratio of 2.97 contained a higher exchangeable site that increased the ion exchange rate. Besides, the crystal size of MOR zeolite is larger than that of LTL crystal, which might decrease the diffusion rate of ion in MOR zeolite as observed in other reported works (Kwon et al. 2020).

Equilibrium studies

The metal ions adsorption in terms of removal efficiency and adsorption capacity were shown in Fig. 4. The removal efficiency of Cu^{2+}, Cd^{2+}, Pb^{2+}, Zn^{2+}, Cs^{+}, Sr^{2+} on LTL and MOR zeolite at initial concentrations ranged from 10 – 600 ppm were shown in Fig. 4a and Fig. 4c, respectively. At the initial concentration of 10 ppm, LTL zeolite effectively removed Cd^{2+}, Pb^{2+}, Sr^{2+} and Cs^{+} with the efficiency of 96, 97.1, 95.4 and 97.6% respectively. At the same time, the removal efficiency of MOR zeolite to Cu^{2+}, Cd^{2+}, Pb^{2+}, Sr^{2+} and Cs^{+} was 98.2, 98.2, 96.9, 94.9 and 99%, respectively. These results revealed that both LTL and MOR zeolites were able to effectively remove these metal ions at low concentration in water. The removal efficiency of both zeolites dramatically decreased with increasing concentration of all metal ions. However, this is a relative number based on the concentration of metal ions before and after adsorption. In high concentration condition, the adsorption capacity is a more important value.

The adsorption capacity of Cu^{2+}, Cd^{2+}, Pb^{2+}, Zn^{2+}, Cs^{+}, Sr^{2+} ions on LTL and MOR zeolites at different initial concentrations ranging from 10 – 600 ppm were presented in Fig. 4b and Fig. 4d, respectively. We observed that in almost all cases of tested metal ions, the adsorption capacity of both LTL and MOR zeolites in removal of metal ions increased with increasing concentration of metal ions. The same result was reported by the previous study on the adsorption of Zn^{2+} in natural zeolite. The adsorption capacity of Zn^{2+} increased with the increase of initial concentration until the saturation point reached. At that point, the further increase of the metal ions concentration would not result in any significant change in adsorption capacity. The increase of Zn^{2+} amount created the concentration gradient and driving force to uptake Zn^{2+} to adsorbent, which was responsible to overcome the mass transfer resistance associated with the adsorption of metal ions from solution by zeolite (Zendelska et al. 2014).

In our study, the saturated point of the adsorption of Cu^{2+}, Cd^{2+}, Zn^{2+}, Sr^{2+} on LTL zeolite was established at the initial metal ions concentration of 50 ppm. The further increased concentration to 100 ppm led to a slight increase in the uptake capacity, but it was not significant. The maximum obtained values in adsorption capacity were 28.3, 43.9, 23.1 and 34.6 mg/g for Cu^{2+}, Cd^{2+}, Zn^{2+} and Sr^{2+}, respectively. In the adsorption of Pb^{2+} and Cs^{+} metal ions in LTL zeolite, the saturated points were obtained at initial concentration of 100 ppm and 450 ppm with the highest adsorption capacity of 141.4 mg/g and 278.8 mg/g, respectively. In the case of Pb^{2+} ions, the uptake capacity of LTL zeolite was almost unchanged with further increase in solution concentration. However, the adsorption capacity of LTL zeolite for both Cs^{+} and Pb^{2+} ions decreased as the initial concentration increased to 600 ppm (Fig. 4b). The obtained result might be due to the microstructure and the affinity of LTL zeolite to Cs^{+} and Pb^{2+} in the adsorption of these metals ions. It was known that the metal ion uptake by zeolite adsorbent occurred by the combination of ion-exchange and adsorption process. Metal ions had to move to the zeolite surface and the pore windows. In the next state, metal ions migrated and diffused through the channel systems to ion-exchange sites and replaced the exchangeable ions (Erdem et al. 2004). In this study, LTL zeolite is a large pore and one-dimension channel system running along the *c*-axis of cylindrical type crystal. In addition, the as-synthesized LTL with Si/Al ratio of 2.97 was relatively low. It created a high concentration of ion-exchange sites in the framework. Due to these microstructure properties, at high concentration of metal ions containing high density of metal ions in solution, metal ions rapidly contacted and occupied the exchangeable sites in the channels near the crystal surface. As a result, the first occupied ions blocked the channel window and prevented the further diffusion of metal ions in the aqueous solution into the LTL zeolite channel, resulting in decrease of adsorption capacity.

In comparison, in this study the as-synthesized MOR zeolite had Si/Al ratio of 6.91 and 2-dimensional channel system. The adsorption of metal ions occurred relatively slower. The adsorption of Cu^{2+} and Sr^{2+} ions reached a saturated point at initial concentration of 50 and 150 ppm and the highest adsorption capacity was 41.3 and 83.3 mg/g, respectively. With continuously increasing the concentration of metal ions to 600 ppm, the adsorption of Zn^{2+}, Cd^{2+}, Pb^{2+} on MOR zeolite was saturated. The maximum adsorption capacity was 71.8 mg/g of Zn^{2+}, 131.9 mg/g of Cd^{2+} and 178.9 mg/g of Pb^{2+}. The uptake of Cs^{+} ions in MOR zeolite in this study has not reached a saturated point at this state. The uptake capacity gradually increased with increasing the initial concentration of Cs^{+} ions in solution (Fig. 4d). The adsorption capacity obtained at initial concentration of 600 ppm was 238.8 mg/g of Cs^{+} which is lower than the highest adsorption capacity of LTL zeolite to Cs^{+}.

Interestingly, we observed in the case of Pb^{2+} adsorption in both LTL and MOR zeolites, the highest uptake amount of Pb^{2+} to LTL zeolite was 141 mg/g corresponding to 85% compared to that of MOR zeolite (179 mg/g) although the ion exchange site in LTL zeolite was almost twice to MOR zeolite. We conducted the EDS measurement on the Pb^{2+} saturated adsorbed on both zeolites and found that 60% of exchangeable sites in LTL zeolite remained (4.74% in 7.99%) whilst all Na^{+} in exchange sites were replaced by Pb^{2+} in MOR zeolite (3.86%) as shown in Table 4. This obtained result is consistent with the adsorption capacity curves for Pb^{2+} ions in Figure 4b and Figure 4d. And it also revealed that the microstructure of zeolite in this study strongly affected metal ion uptake.

We observed that the adsorption capacities of both LTL and MOR zeolite to Cs^{+} and Pb^{2+} ions were relatively higher compared to the result obtained from the remaining metal ions. These results might be due to the effect of ionic radius, hydrated radius and hydration energy of the metal ions to the adsorption process. It was reported that, the adsorption of metal ions to microporous materials depended on the hydrated radius and hydration energy of metal ions. In fact, in a solution with pH value at about 6.5 or lower, metal ions existed as a hydrated state. As a result, the ions with smaller ionic radius could closely attack to the adsorbent surface and easily enter the channels of the adsorbent. Furthermore, the low hydration energy ions could easily be dehydrated and shrink in size for better adsorption (Sounthararajah et al. 2015). In our study, Cs^{+} and Pb^{2+} ions have hydrated radius smaller than the pore diameter of LTL and MOR zeolite beside the lower hydrated energy compared to that of remaining ions as listed in Table 5. These factors responded to the experiment result that LTL and MOR zeolite showed higher adsorption capacity to Cs^{+} and Pb^{2+} metal ions. The highest hydration energy of Cu^{2+} and Zn^{2+} could also relate to their low adsorption capacity on both zeolites.

Sorption modeling

Kinetic model: The adsorption kinetic was modelled by applying pseudo-first-order and pseudo-second-order rate models. The Lagergren first-order rate model can be described as equation (3) (Ho and McKay 1999b)

$$log\,(q_e - q_t) = log\,(q_e) - \frac{k_1}{2.303}t \qquad (3)$$

The Lagergren second-order rate model can be described as equation (4)

$$\frac{t}{q_t} = \frac{1}{k_2 q_e^2} + \frac{t}{q_e} \qquad (4)$$

where q_t (mg/g) is the amount of adsorbed metal ions per unit weight of zeolite at time "t" (min), q_e (mg/g) is the amount of adsorbed metal ions at equilibrium, k_1 (1/min) is the

equilibrium rate constant of pseudo-first sorption, calculated from the slope of the linear regression equation of $\log(q_e-q_t)$ on $\log(q_e)$, k_2 (g/mg.min) is the equilibrium rate constant of pseudo-second sorption, calculated from the intercept of the linear regression equation of t/q_t on t/q_e. The fitted degree of the isotherm and kinetic models to experimental data was investigated by the correlation coefficient R^2.

Isotherm model: The equilibrium metal adsorption data was simulated with the Langmuir and Freundlich models. Langmuir sorption isotherm bases on the monolayer coverage of the sorbent surface and assumes that sorption occurs at specific homogenous sorption sites. All the sorption sites are energetically identical and intermolecular forces decrease rapidly with the distance from the sorption surface (El-Kamash 2008).

The Langmuir model can be described as equation (5) (El-Kamash 2008)

$$\frac{C_e}{q_e} = \frac{1}{Q^0 K_L} + \frac{C_e}{Q^0} \qquad (5)$$

where q_e (mg/g) is the amount of metal ions adsorbed by unit weight of zeolite, C_e (mg/L) is the equilibrium concentration of metal ions in the solution, Q^0 (mg/g) is the monolayer adsorption capacity and K_L is the Langmuir constant related to the free energy of adsorption. Q^0 and K_L are calculated from the slope and the intercept of the linear regression equation of C_e/q_e on C_e.

The characteristic of the Langmuir isotherm model is expressed by the equilibrium parameter R_L

$$R_L = \frac{1}{1 + K_L C_0} \qquad (6)$$

where C_0 is the highest initial metal ions concentration (mg/L). The value of R_L indicates the type of isotherm adsorption to be irreversible ($R_L = 0$), favorable ($0 < R_L < 1$), linear ($R_L = 1$), or unfavorable ($R_L > 1$) (El-Kamash 2008).

The Freundlich isotherm model describes the multilayer sorption on heterogeneous surfaces. This isotherm expresses the surface heterogeneity and the exponential distribution of active sites and their energy (El-Kamash 2008). The Freundlich model can be described as equation (7)

$$\log(q_e) = \log(K_F) + \frac{1}{n}\log(C_e) \qquad (7)$$

where q_e (mg/g) is the amount of adsorbed metal ions per unit weight of zeolite, C_e (mg/L) is the equilibrium concentration of metal ions in the solution, K_F is Freundlich

constant indicating the relative sorption capacity of adsorbent, and 1/n is the constant indicating the intensity of the sorption process. K_F and n are calculated from the slope and the intercept of the linear regression equation of $\log(q_e)$ on $\log(C_e)$ (El-Kamash 2008).

The adsorption isotherm modelling of metal ions on LTL and MOR zeolites were plotted in Fig. 5. The obtained result showed that the adsorption of tested metal ions fitted to Langmuir model with higher fitting degree compared to Freundlich model as shown in Fig. 5a,c and Fig. 5b,d, respectively and the correlation coefficients R^2 of these equations in Table 6. The monolayer adsorption capacity Q^0 values calculated from Langmuir model (Table 6) were relevant to that obtained from experimental data. The results revealed that the adsorption of metal ions on both LTL and MOR zeolites were monolayer and chemical interaction to homogenous adsorption sites. The values of equilibrium parameter R_L for the adsorption of all metal ions on both zeolites were between 0 and 1 (Table 6), indicating the favorable adsorption of metal ions on these zeolites.

Conclusion

We have reported herein the synthesis of two large pore zeolites as LTL and MOR zeolite by conventional hydrothermal reaction. The as-synthesized zeolites were used to adsorb heavy metal ions including Cu^{2+}, Cd^{2+}, Pb^{2+}, Zn^{2+} and radioactive ions as Cs^{+} and Sr^{2+}. At low concentration of metal ions, LTL and MOR showed efficient removal of the tested metal ions. In solution with high concentration of metal ions, the adsorption kinetic followed the pseudo-second-order model indicating the chemisorption process of metal ions on both LTL and MOR zeolites. The results, fitted well to the Langmuir isotherm model, revealed the monolayer adsorption on homogenous surfaces of LTL and MOR zeolite. The equilibrium adsorption results showed that the microstructure of zeolite significantly affected the adsorption capacity of LTL and MOR zeolite on removal of tested metal ions. Both LTL and MOR showed highest adsorption capacity for Cs^{+} and Pb^{2+} metal ions.

Declarations

Ethics approval and consent to participate: Not applicable.

Consent for publication: Not applicable.

Availability of data and materials: All data generated or analysed during this study are included in this published article.

Financial interests: The authors declare they have no financial interests.

Competing interests: The authors declare that they have no competing interests.

Funding: This work was supported by Vietnam National University, Ho Chi Minh City, Vietnam for project code No. C2018-18-23.

Authors' contributions: D.H-P.N designed and conducted experiments on zeolite synthesis, metal adsorption, and manuscript preparation. **Q.T.L** carried out the material characterization. **T.C-T.P**, **T.T.L** designed experiments, supervisor, and project administration, prepared-wrote and edited the manuscript.

References

Aghel B, Mohadesi M, Gouran A, Razmegir MH (2020) Use of Modified Iranian Clinoptilolite Zeolite for Cadmium and Lead Removal from Oil Refinery Wastewater. Int J Environ Sci Technol. https://doi.org/10.1007/s13762-019-02466-5

Azimi A, Azari A, Rezakazemi M, Ansarpour M (2017) Removal of Heavy Metals from Industrial Wastewaters: A Review. ChemBioEng Rev 4:37–59. https://doi.org/10.1002/cben.201600010

Calzaferri G (2020) Nanochannels of Zeolite L. In: Martínez-Martínez V, López Arbeloa F (eds) Dyes and Photoactive Molecules in Microporous Systems. Springer International Publishing, Cham, pp 48–49.

Collins F, Rozhkovskaya A, Outram JG, Millar GJ (2020) A Critical Review of Waste Resources, Synthesis, and Applications for Zeolite LTA. Microporous Mesoporous Mater 291:109667. https://doi.org/10.1016/j.micromeso.2019.109667

Datta SJ, Moon WK, Choi DY, Hwang IC, Yoon KB (2014) A Novel Vanadosilicate with Hexadeca-Coordinated Cs^+ Ions as a Highly Effective Cs^+ Remover. Angew Chemie Int Ed 53:7203–7208. https://doi.org/10.1002/anie.201402778

Datta SJ, Oleynikov P, Moon WK, Ma Y, Mayoral A, Kim H, Dejoie C, Song MK, Terasaki O, Yoon KB (2019) Removal of ^{90}Sr from Highly Na^+-rich Liquid Nuclear Waste With a Layered Vanadosilicate. Energy Environ Sci 12:1857–1865. https://doi.org/10.1039/C8EE03302A

Davis ME (2014) Zeolites from a Materials Chemistry Perspective. Chem Mater 26:239–245. https://doi.org/10.1021/cm401914u

El-Kamash AM (2008) Evaluation of Zeolite A for the Sorptive Removal of Cs^+ and Sr^{2+} Ions from Aqueous Solutions Using Batch and Fixed Bed Column Operations. J Hazard Mater 151:432–445. https://doi.org/10.1016/j.jhazmat.2007.06.009

El-Kamash AM, Zaki AA, El Geleel MA (2005) Modeling Batch Kinetics and Thermodynamics of Zinc and Cadmium Ions Removal from Waste Solutions Using Synthetic Zeolite A. J Hazard Mater 127:211–220. https://doi.org/10.1016/j.jhazmat.2005.07.021

Erdem E, Karapinar N, Donat R (2004) The Removal of Heavy Metal Cations by Natural Zeolites. J Colloid Interface Sci 280:309–314. https://doi.org/10.1016/j.jcis.2004.08.028

Fois E, Tabacchi G, Devaux A, Belser P, Brühwiler D, Calzaferri G, (2013) Host–Guest

Interactions and Orientation of Dyes in the One-Dimensional Channels of Zeolite L. Langmuir 29:9188–9198. https://doi.org/10.1021/la400579w

Galletti C, Dosa M, Russo N, Fino D (2021) Zn^{2+} and Cd^{2+} Removal from Wastewater Using Clinoptilolite as Adsorbent. Environ. Sci. Pollut. Res. 28:24355–24361. https://doi.org/10.1007/s11356-020-08483-z

Günay A, Arslankaya E, Tosun I (2007) Lead Removal from Aqueous Solution by Natural and Pretreated Clinoptilolite: Adsorption Equilibrium and Kinetics. J Hazard Mater 146:362–371. https://doi.org/10.1016/j.jhazmat.2006.12.034

Hincapie BO, Garces LJ, Zhang Q, Sacco A, Suib SL (2004) Synthesis of Mordenite Nanocrystals. Microporous Mesoporous Mater 67:19–26. https://doi.org/10.1016/j.micromeso.2003.09.026

Ho YS, McKay G (1999a) Pseudo-Second Order Model for Sorption Processes. Process Biochem 34:451–465. https://doi.org/10.1016/S0032-9592(98)00112-5

Ho YS, McKay G (1999b) The Sorption of Lead(II) Ions on Peat. Water Res 33:578–584. https://doi.org/10.1016/S0043-1354(98)00207-3

Ibrahim HS, Jamil TS, Hegazy EZ (2010) Application of Zeolite Prepared from Egyptian Kaolin for the Removal of Heavy Metals: II. Isotherm Models. J Hazard Mater 182:842–847. https://doi.org/10.1016/j.jhazmat.2010.06.118

Hong M, Yu L, Wang Y, Zhang J, Chen Z, Dong L, Zan Q, Li R (2019) Heavy Metal Adsorption with Zeolites: The Role of Hierarchical Pore Architecture. Chem Eng J 359:363–372. https://doi.org/10.1016/j.cej.2018.11.087

Kwon S, Choi Y, Singh BK, Na K (2020) Selective and Rapid Capture of Sr^{2+} with LTA Zeolites: Effect of Crystal Sizes and Mesoporosity. Appl Surf Sci 506:145029. https://doi.org/10.1016/j.apsusc.2019.145029

Li J, Li M, Song Q, Wang S, Cui X, Liu F, Liu X (2020) Efficient Recovery of Cu(II) by LTA-zeolites with Hierarchical Pores and Their Resource Utilization in Electrochemical Denitrification: Environmentally Friendly Design and Reutilization of Waste in Water. J Hazard Mater 394:122554. https://doi.org/10.1016/j.jhazmat.2020.122554

Lobo RF (2003) Introduction to the Structural Chemistry of Zeolites. In: Auerbach SM, Carrado KA, Dutta PK (eds) Handbook of Zeolite Science and Technology. Marcel Dekker, pp 62–64.

Lu X, Wang F, Li X, Shih K, Zeng EY (2016) Adsorption and Thermal Stabilization of

Pb^{2+} and Cu^{2+} by Zeolite. Ind Eng Chem Res 55:8767–8773. https://doi.org/10.1021/acs.iecr.6b00896

Marcus Y (1991) Thermodynamics of Solvation of Ions. Part 5.—Gibbs Free Energy of Hydration at 298.15 K. J Chem Soc Faraday Trans 87:2995–2999. https://doi.org/10.1039/FT9918702995

McCusker LB, Olson DH, Baerlocher C (2007) Atlas of Zeolite Framework Types. Elsevier, Amsterdam.

Mihaly-Cozmuta L, Mihaly-Cozmuta A, Peter A, Nicula C, Tutu H, Silipas D, Indrea E (2014) Adsorption of Heavy Metal Cations by Na-clinoptilolite: Equilibrium and Selectivity Studies. J Environ Manage 137:69–80. https://doi.org/10.1016/j.jenvman.2014.02.007

Moattar F, Hayeripour S (2004) Application of Chitin and Zeolite Adsorbents for Treatment of Low Level Radioactive Liquid Wastes. Int J Environ Sci Technol 1:45–50. https://doi.org/10.1007/BF03325815

Nightingale Jr ER (1959) Phenomenological Theory of Ion Solvation. Effective Radii of Hydrated Ions. J Phys Chem 63:1381–1387. https://doi.org/10.1021/j150579a011

Pham TCT, Docao S, Hwang IC, Song MK, Choi DY, Moon D, Oleynikov P, Yoon KB (2016) Capture of Iodine and Organic Iodides Using Silica Zeolites and the Semiconductor Behaviour of Iodine in a Silica Zeolite. Energy Environ Sci 9:1050–1062. https://doi.org/10.1039/C5EE02843D

Prajitno MY, Tangparitkul S, Zhang H, Harbottle D, Hunter TN (2021) The Effect of Cationic Surfactants on Improving Natural Clinoptilolite for the Flotation of Cesium. J Hazard Mater 402:123567. https://doi.org/10.1016/j.jhazmat.2020.123567

Shen X, Qiu G, Yue C, Guo M, Zhang M (2017) Multiple Copper Adsorption and Regeneration by Zeolite 4A Synthesized from Bauxite Tailings. Environ Sci Pollut Res. https://doi.org/10.1007/s11356-017-9824-5

Sounthararajah DP, Loganathan P, Kandasamy J, Vigneswaran S (2015) Adsorptive Removal of Heavy Metals from Water Using Sodium Titanate Nanofibres Loaded onto GAC in Fixed-bed Columns. J Hazard Mater 287:306–316. https://doi.org/10.1016/j.jhazmat.2015.01.067

Sprynskyy M, Buszewski B, Terzyk AP, Namieśnik J (2006) Study of the Selection Mechanism of Heavy Metal (Pb^{2+}, Cu^{2+}, Ni^{2+}, and Cd^{2+}) Adsorption on

Clinoptilolite. J Colloid Interface Sci 304:21–28. https://doi.org/10.1016/j.jcis.2006.07.068

Tashauoei HR, Attar HM, Amin MM, Kamali M, Nikaeen M, Dastjerdi MV (2010) Removal of Cadmium and Humic Acid from Aqueous Solutions Using Surface Modified Nanozeolite A. Int J Environ Sci Technol. https://doi.org/10.1007/BF03326159

Wang S, Terdkiatburana T, Tadé MO (2008) Adsorption of Cu(II), Pb(II) and Humic Acid on Natural Zeolite Tuff in Single and Binary Systems. Sep Purif Technol 62:64–70. https://doi.org/10.1016/j.seppur.2008.01.004

Zendelska A, Golomeova M, Blažev K, Krstev B, Golomeov B, Krstev A (2014) Kinetic Studies of Zinc Ions Removal from Aqueous Solution by Adsorption on Natural Zeolite. Int J Sci Environ Technol 3:1303–1318

Caption to Figures and Tables

Fig. 1 Characterization of adsorbents, SEM image and XRD pattern of synthesized LTL zeolite (a,b) and MOR zeolite (c,d).

Fig. 2 Plots of experimental data and kinetic modelling of the metal ion adsorption on LTL zeolite including a) Cs^{+}, b) Pb^{2+}, c) Cd^{2+}, d) Sr^{2+}, e) Cu^{2+}, f) Zn^{2+}, g) pseudo-first-order model, h) pseudo-second-order model with different period of adsorption time.

Fig. 3 Plots of experimental data and kinetic modelling of the metal ion adsorption on MOR zeolite including a) Cs^{+}, b) Pb^{2+}, c) Cd^{2+}, d) Sr^{2+}, e) Cu^{2+}, f) Zn^{2+}, g) pseudo-first-order model, h) pseudo-second-order model with different period of adsorption time.

Fig. 4 Metal ion adsorption in term of removal efficiency and adsorption capacity of metal ions on LTL zeolite (a and b) and MOR zeolite (c and d) with different initial concentration of metal ions.

Fig. 5 The adsorption modelling of metal ions on LTL (a, b) and MOR zeolite (c, d) with Langmuir isotherm model (a, c) and Freundlich isotherm model (b, d), respectively.

Table 1 Parameters of pseudo-first-order and pseudo-second-order models for the adsorption of Cu^{2+}, Cd^{2+}, Pb^{2+}, Zn^{2+}, Cs^{+}, Sr^{2+} on LTL zeolite

Table 2 Parameters of pseudo-first-order and pseudo-second-order models for the adsorption of Cu^{2+}, Cd^{2+}, Pb^{2+}, Zn^{2+}, Cs^{+}, Sr^{2+} on MOR zeolite

Table 3 Pseudo-second-order rate constant of the metal ion adsorption on synthesized LTL and MOR zeolites.

Table 4 EDS measurement data of Pb^{2+} saturated adsorbed on LTL and MOR zeolite.

Table 5 Ionic radius, hydrated radius and hydration energy of metal ions in this study.

Table 6 Parameters of Langmuir and Freundlich models for the adsorption of Cu^{2+}, Cd^{2+}, Pb^{2+}, Zn^{2+}, Cs^{+}, Sr^{2+} on LTL and MOR zeolite

Fig. 1

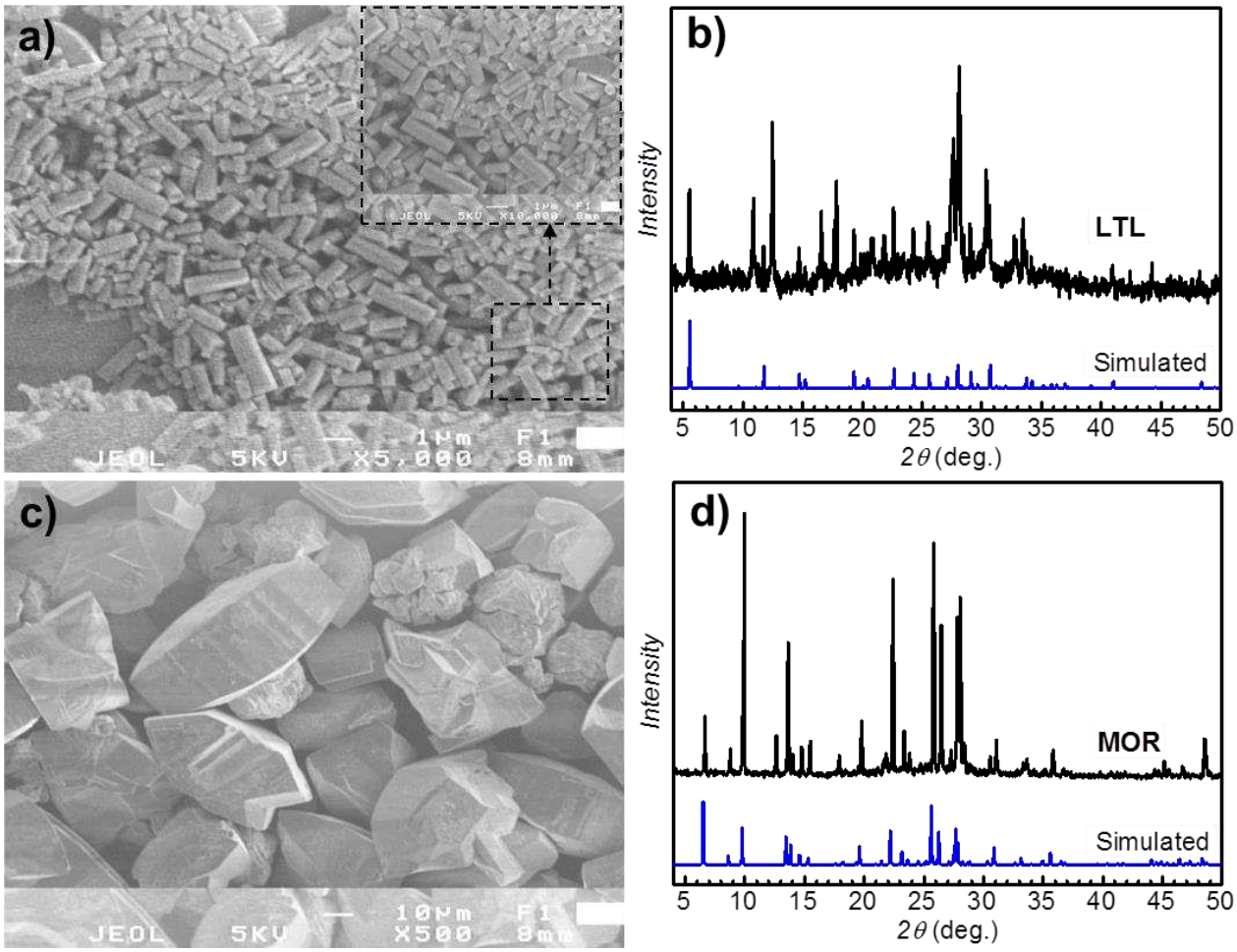
a)
JEOL 5KV X5,000 8mm
b)
Intensity
LTL
Simulated
5 10 15 20 25 30 35 40 45 50
2θ (deg.)
c)
JEOL 5KV X500 8mm
d)
Intensity
MOR
Simulated
5 10 15 20 25 30 35 40 45 50
2θ (deg.)

Fig. 2

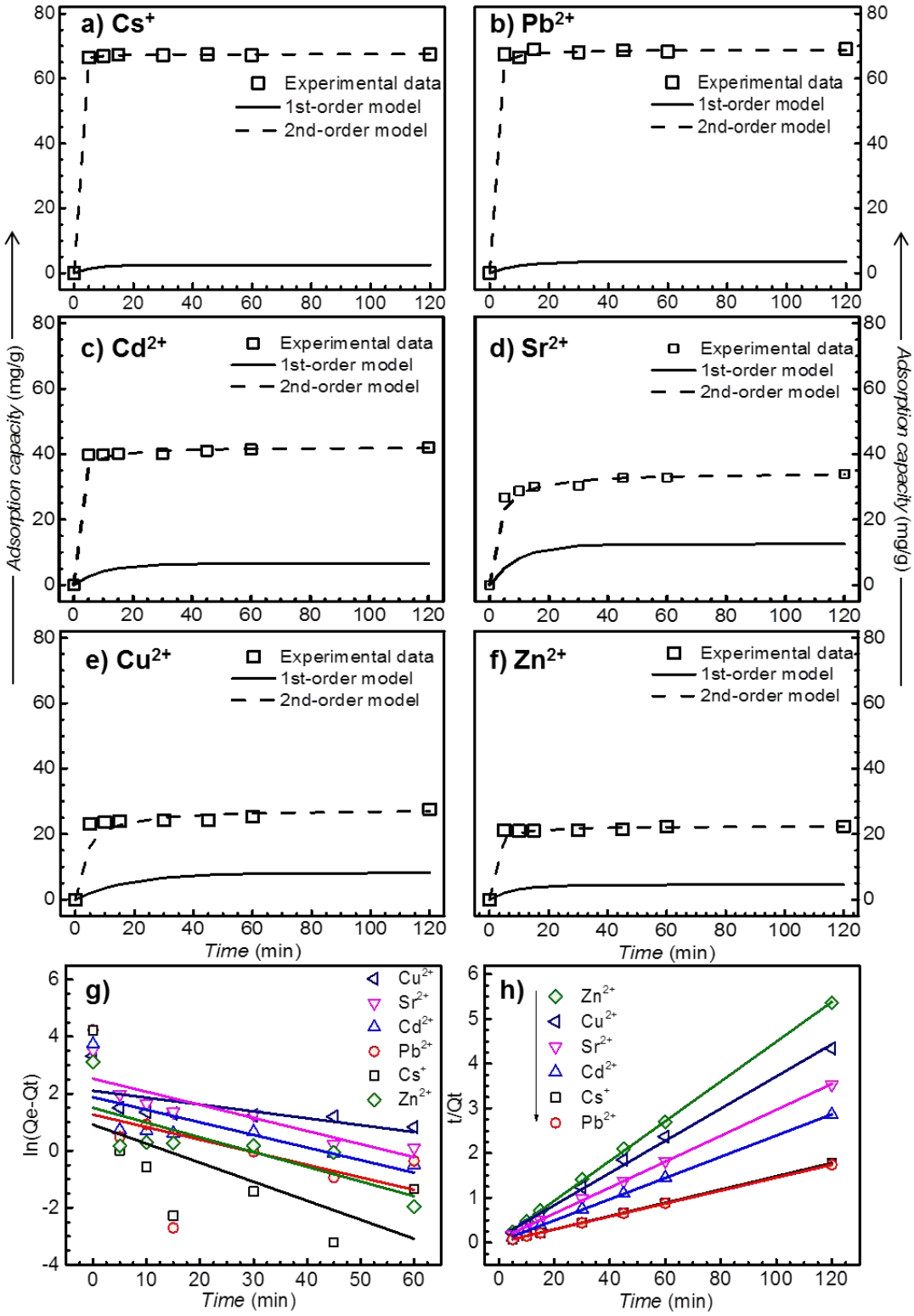
a) Cs+
b) Pb2+
c) Cd2+
d) Sr2+
e) Cu2+
f) Zn2+
Experimental data
1st-order model
2nd-order model
Adsorption capacity (mg/g)
Time (min)
g)
h)
ln(Qe-Qt)
t/Qt
Cu2+
Sr2+
Cd2+
Pb2+
Cs+
Zn2+

Fig. 3

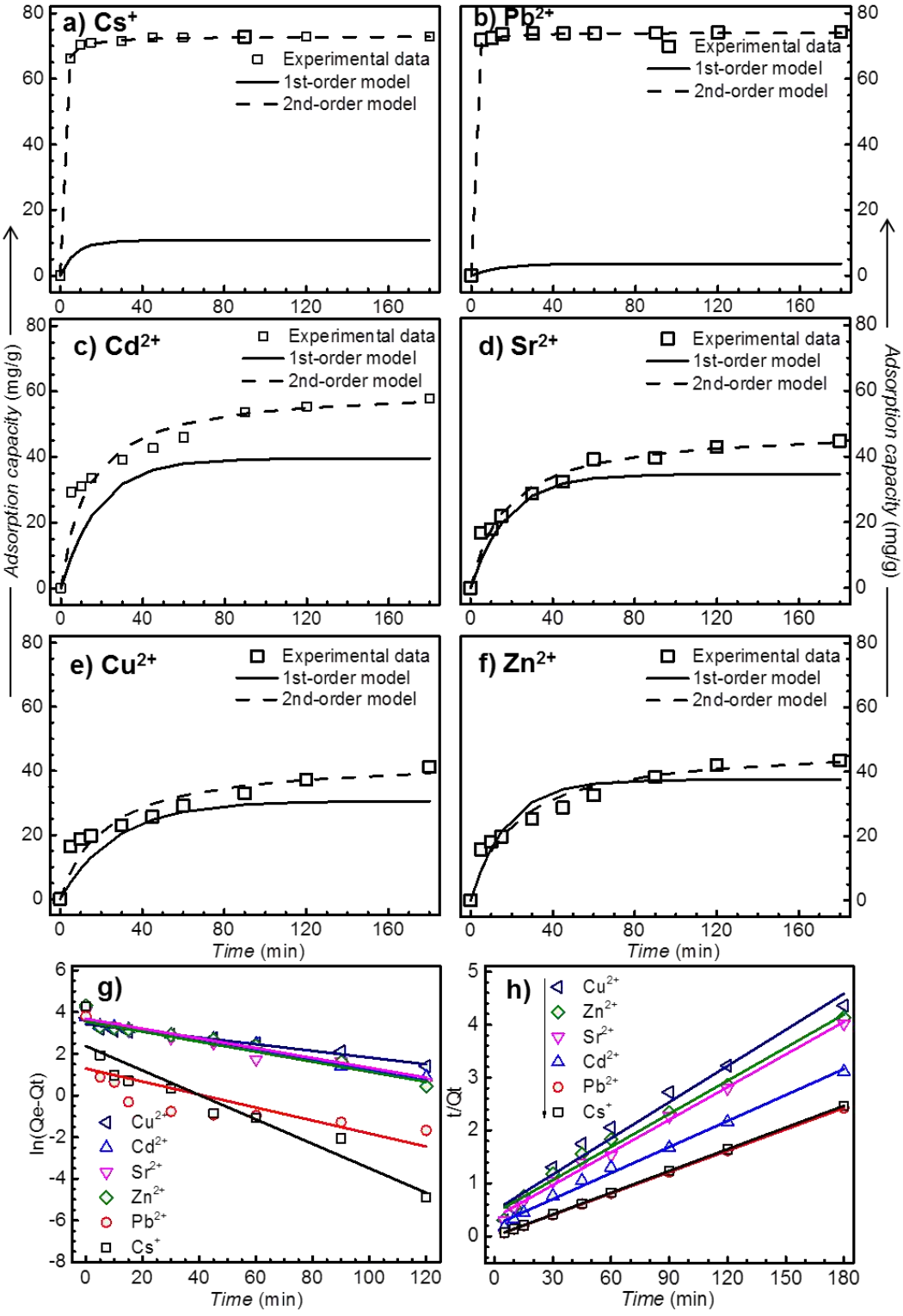
a) Cs+
b) Pb2+
c) Cd2+
d) Sr2+
e) Cu2+
f) Zn2+
Experimental data
1st-order model
2nd-order model
Adsorption capacity (mg/g)
Time (min)
g)
ln(Qe-Qt)
Cu2+
Cd2+
Sr2+
Zn2+
Pb2+
Cs+
h)
t/Qt
Time (min)

Fig. 4

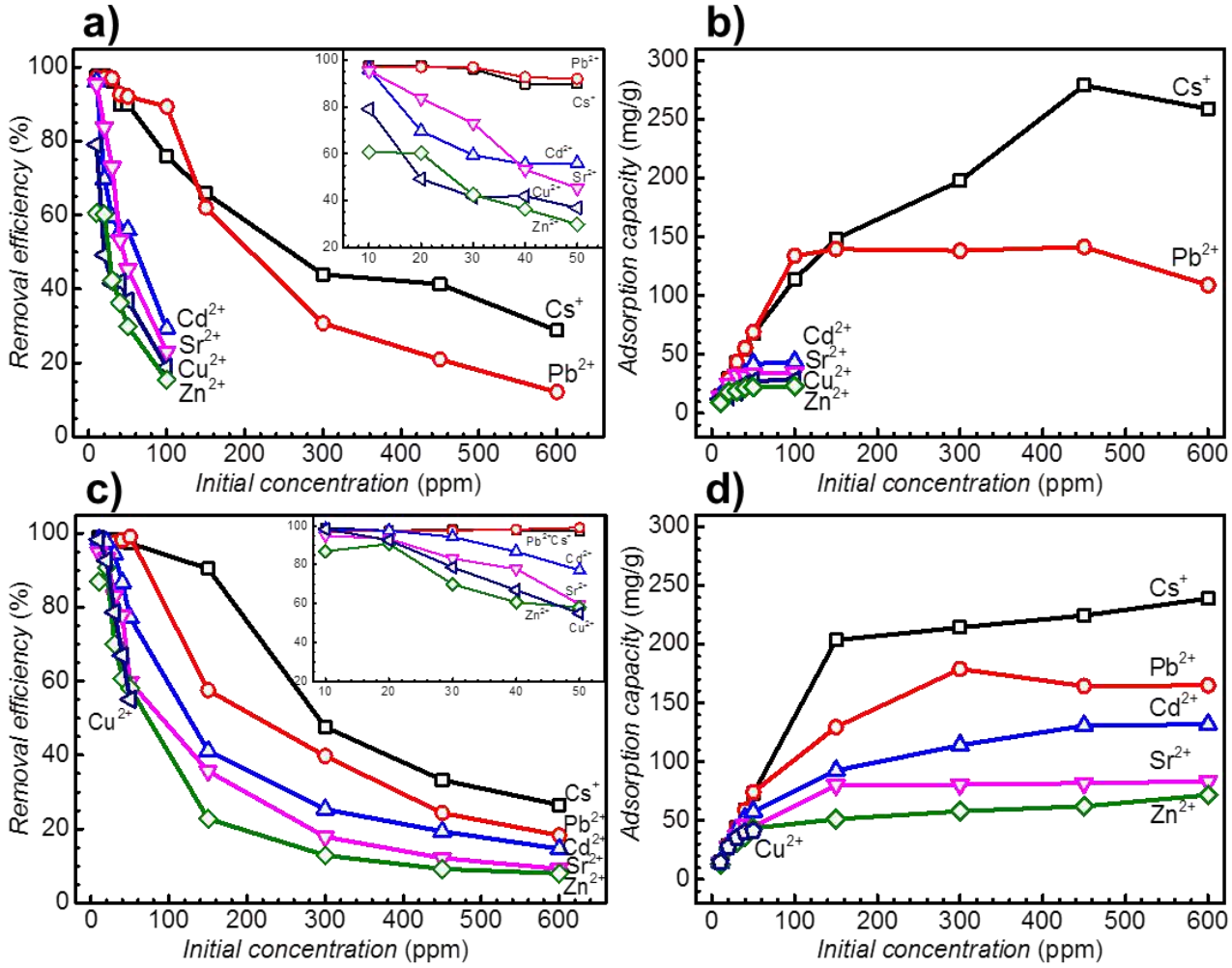
a)
b)
c)
d)
Removal efficiency (%)
Adsorption capacity (mg/g)
Initial concentration (ppm)
Cs+
Pb2+
Cd2+
Sr2+
Cu2+
Zn2+

Fig. 5

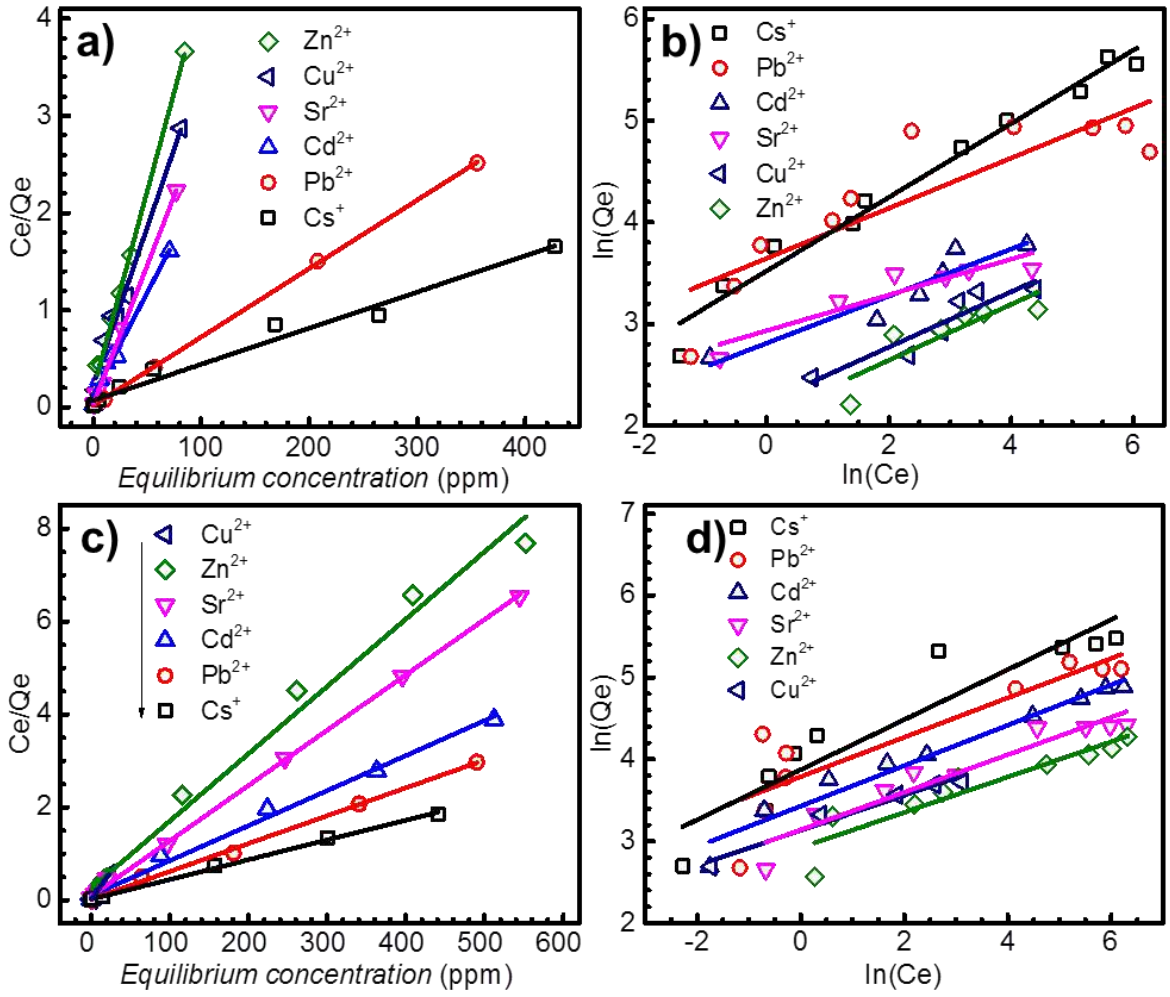
a)
Zn2+
Cu2+
Sr2+
Cd2+
Pb2+
Cs+
Ce/Qe
Equilibrium concentration (ppm)
b)
Cs+
Pb2+
Cd2+
Sr2+
Cu2+
Zn2+
ln(Qe)
ln(Ce)
c)
Cu2+
Zn2+
Sr2+
Cd2+
Pb2+
Cs+
Ce/Qe
Equilibrium concentration (ppm)
d)
Cs+
Pb2+
Cd2+
Sr2+
Zn2+
Cu2+
ln(Qe)
ln(Ce)

Table 1

Metal ion	Cu^{2+}	Cd^{2+}	Pb^{2+}	Zn^{2+}	Cs^{+}	Sr^{2+}
Pseudo-first-order model						
$q_{es}^{(a)}$(mg/g)	8.2	6.6	3.6	4.5	2.5	12.5
$k_1^{(b)}$ (1/min)	0.056	0.102	0.101	0.119	0.153	0.105
Correlation coefficient R^2	0.4366	0.5227	0.2142	0.6047	0.3860	0.7871
Pseudo-second-order model						
$q_{es}^{(a)}$(mg/g)	27.8	42.2	69.0	22.5	67.6	34.5
$k_2^{(c)}$(g/mg.min)	0.0111	0.0281	0.0501	0.0407	0.1685	0.0120
Correlation coefficient R^2	0.9966	0.9999	1	0.9997	1	0.9995
$q_e^{(d)}$ (mg/g)	27.6	42.0	69.1	22.4	67.5	34.0

(^{a}) simulated equilibrium adsorption capacity, (^{b}) pseudo-first sorption rate constant, (^{c}) pseudo-second sorption rate constant, ^{d}) experimental adsorption capacity

Table 2

Metal ion	Cu^{2+}	Cd^{2+}	Pb^{2+}	Zn^{2+}	Cs^{+}	Sr^{2+}
Pseudo-first-order model						
$q_{es}^{(a)}$(mg/g)	30.6	39.5	3.6	37.6	10.7	34.6
$k_1^{(b)}$ (1/min)	0.037	0.054	0.072	0.056	0.135	0.056
Correlation coefficient R^2	0.9538	0.9609	0.5017	0.9681	0.8843	0.9649
Pseudo-second-order model						
$q_{es}^{(a)}$(mg/g)	43.9	61.0	74.1	48.1	73.0	48.5
$k_2^{(c)}$(g/mg.min)	0.0011	0.0013	0.0552	0.0010	0.0284	0.0012
Correlation coefficient R^2	0.9774	0.9936	1	0.9884	1	0.9955
$q_e^{(d)}$ (mg/g)	41.3	57.8	74.3	43.6	73.0	44.8

$^{(a)}$ simulated equilibrium adsorption capacity, $^{(b)}$ pseudo-first sorption rate constant, $^{(c)}$ pseudo-second sorption rate constant, $^{(d)}$ experimental adsorption capacity

Table 3

Zeolite	Rate constant $k_2 \times 10^3$ (g/mg.min)					
	Pb^{2+}	Cu^{2+}	Cs^{+}	Sr^{2+}	Zn^{2+}	Cd^{2+}
LTL	50.1	11.1	168.5	12	40.7	28.1
MOR	55.2	1.1	28.4	1.2	1.0	1.3

Table 4

Element	LTL zeolite (Atomic%)		MOR zeolite (Atomic%)	
	Before adsorption	After adsorption	Before adsorption	After adsorption
O	69.23	63.37	68.86	69.03
Al	6.25	7.99	3.45	3.86
Si	18.57	22.18	23.83	25.18
K	5.95	4.74	-	-
Na	-	-	3.86	0
Pb	0	1.72	0	1.93

Table 5

Metal ion	Ionic radius (Nightingale Jr 1959) (nm)	Hydrated radius (Nightingale Jr 1959) (nm)	Hydration energy (Marcus 1991) (kJ/mol)
Cs^{+}	0.169	0.329	-245
Pb^{2+}	0.132	0.410	-1,345
Sr^{2+}	0.113	0.412	-1,385
Cu^{2+}	0.072	0.419	-1,920
Cd^{2+}	0.097	0.426	-1,575
Zn^{2+}	0.074	0.430	-1,880

Table 6

Metal ion	Cu^{2+}	Cd^{2+}	Pb^{2+}	Zn^{2+}	Cs^{+}	Sr^{2+}
LTL zeolite						
Langmuir model						
Q^0 (mg/g) [(a)]	30.9	47.2	142.9	24.4	270.3	35.0
K_L (1/g) [(b)]	0.141	0.182	0.372	0.233	0.051	1.007
R_L[(c)]	0.0663	0.0520	0.0045	0.0411	0.0304	0.0098
R^2	0.9841	0.9842	0.9998	0.9975	0.9804	0.9997
Freundlich model						
1/n [(d)]	0.27	0.23	0.25	0.27	0.36	0.18
K_F (mg/g) [(e)]	9.29	16.82	38.32	8.13	33.89	18.82
R^2	0.8675	0.8956	0.7558	0.7271	0.9748	0.8533
q_{max}[(f)] (mg/g)	28.3	43.9	141.4	23.1	278.8	34.6
MOR zeolite						
Langmuir model						
Q^0 (mg/g) [(a)]	42.4	133.3	166.7	69.0	232.6	84.0
K_L (1/g) [(b)]	1.35	0.08	0.35	0.06	0.23	0.14
R_L[(c)]	0.0146	0.0205	0.0047	0.0284	0.0071	0.0118
R^2	0.9986	0.9942	0.9982	0.9876	0.9983	0.9995
Freundlich model						
1/n [(d)]	0.21	0.25	0.24	0.22	0.31	0.23
K_F (mg/g) [(e)]	22.92	30.85	44.16	18.55	48.10	23.12
R^2	0.9666	0.9635	0.7698	0.8682	0.8822	0.9138
q_{max}[(f)] (mg/g)	41.3	131.9	178.9	71.8	238.8	83.3

[(a)] monolayer adsorption capacity, [(b)] Langmuir constant, [(c)] equilibrium parameter, [(d)] sorption intensity constant, [(e)] Freundlich constant, [(f)] experimental maximum adsorption capacity